

Grain-boundary sliding during diffusional creep

E. H. AIGELTINGER, R. C. GIFKINS

Commonwealth Scientific and Industrial Research Organization, University of Melbourne, Victoria 3052, Australia

Grain-boundary sliding and diffusional changes at grain boundaries were monitored on the surface and in the interior of a magnesium alloy Magnox ZR55 tested under diffusional creep conditions. The behaviour is compared and contrasted to that observed under recovery creep conditions. It was found (i) that diffusional and recovery creep exhibit distinctively different angular dependencies of grain-boundary sliding, (ii) that the surface and interior grains exhibit the same sliding and diffusional changes (in the plane of the surface) under diffusional creep conditions, (iii) that a previously presented method for the measurement of diffusional creep [1], when modified as described here, allows the determination of diffusional and sliding components for samples with either as-cut or annealed surface conditions and (iv) that under diffusional creep conditions the value of γ is 0.5.

1. Introduction

Although it is widely recognized that diffusional creep (DC) involves some form of accommodating grain-boundary sliding (GBS) there has been little metallography and no quantitative work on this aspect of creep. A recently proposed method of analysis of marker line offsets [1] allows the determination of diffusional and sliding components at individual grain boundaries. This method has been applied to the magnesium alloy Magnox ZR55 (Mg 0.55 wt% Zr), tested under conditions which give DC and also which result in dislocation creep, probably recovery creep (RC), and the results are presented here. Magnox ZR55 has the advantage that the zirconium hydride stringers (the hydride is formed by annealing in hydrogen) can be used as marker lines to measure GBS in the interior of the material. The diffusional component is also revealed as hydride-free zones on either side of the grain boundaries where magnesium "plates out" during creep.

It has been suggested by Gifkins and Langdon [2] that it should be possible to distinguish between GBS under DC and RC conditions through the dependence of GBS upon the angle θ between a grain-boundary trace and the stress axis.

The results obtained here show this to be the case.

The results also permit calculation of γ , the contribution of GBS to the overall deformation. The theoretical value of γ in the case of DC has been the subject of recent debate [3-5].

The previously proposed marker-line analysis [1] is dependent upon the assumption that grain boundaries incident on the sample surface move during creep from the random "as-cut" configuration to an "annealed" one, so that they become practically normal to the surface. The presence of the hydride precipitate prevents this movement in the Magnox ZR55 and it was, therefore, necessary to modify the analysis to allow for this feature. Details of the modified analysis are also presented here.

The basic measurements reported here are of sliding and diffusional displacements of sets of marker lines on the specimen surface or of the hydride stringers in the interior, together with the widths of the hydride-free zones, all as a function of θ .

Several other measurements were necessary in order to separate the sliding and diffusional components to allow valid comparisons between the two kinds of creep, to allow calculation of γ and

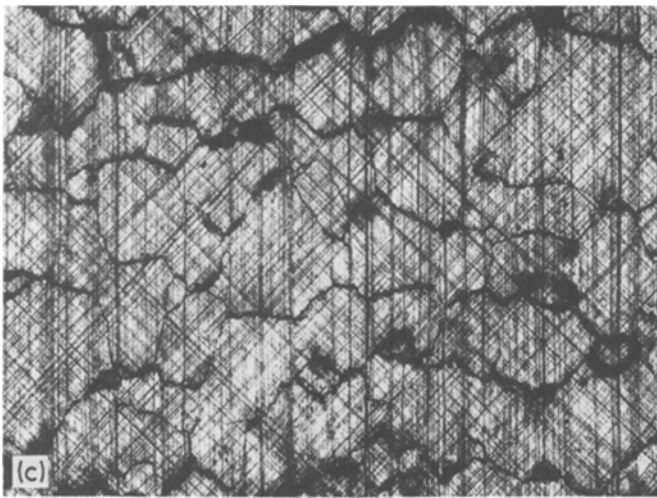
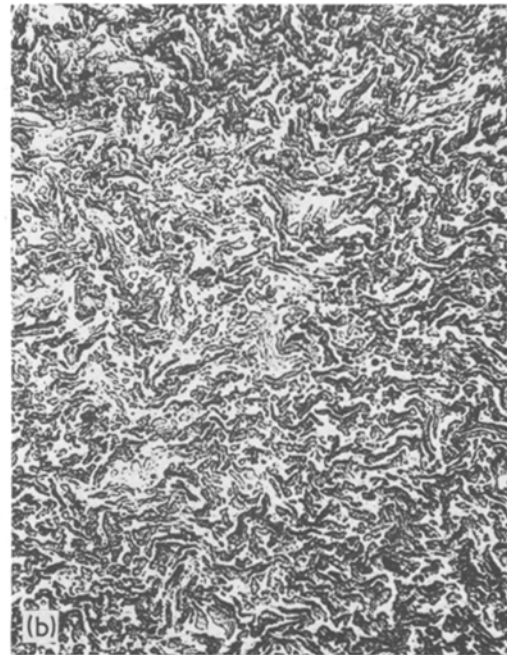
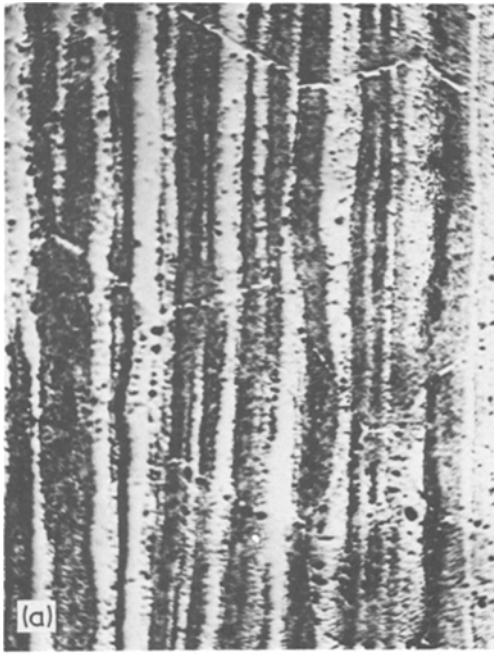


Figure 1 (a) As annealed, parallel to extrusion direction; etched, $\times 368$. (b) As annealed, perpendicular to extrusion direction; etched, $\times 160$. (c) Surface, RC specimen after creep; stress axis vertical; unetched, $\times 96$. (d) Polished and etched section. DC specimen after creep, stress axis vertical; $\times 160$. (e) as (d) RC specimen; $\times 160$.

to indicate the degree of anisotropy of the grain structure.

The measurements required were (i) of v , the displacement due to sliding normal to the specimen surface as a function of θ , (ii) of the grain shape, by determining the frequency of occurrence of values of θ and by the ratio of grain length to grain width (L/W); and (iii) of the angles between grain-boundary traces (the boundary dihedrals) after creep.

2. Experimental procedure and results

2.1. Materials and methods

As already mentioned, Magnox ZR55 has experi-
1890

mental advantages for the measurements proposed; however, it was chosen because it was essential for the material to maintain a stable grain structure during diffusional creep to 5 to 10% strain. Preliminary experiments with OFHC copper led to abandoning this material because of unacceptable grain growth. This was unfortunate, since it was hoped to link the sliding measurements with the work of Burton and Greenwood [6], who measured the stress and temperature dependence of copper in the DC and RC regimes.

The Magnox ZR55 alloy, obtained from Magnesium Elektron, Ltd in 9/16 in. diameter extruded bar, was annealed in flowing dry hydro-

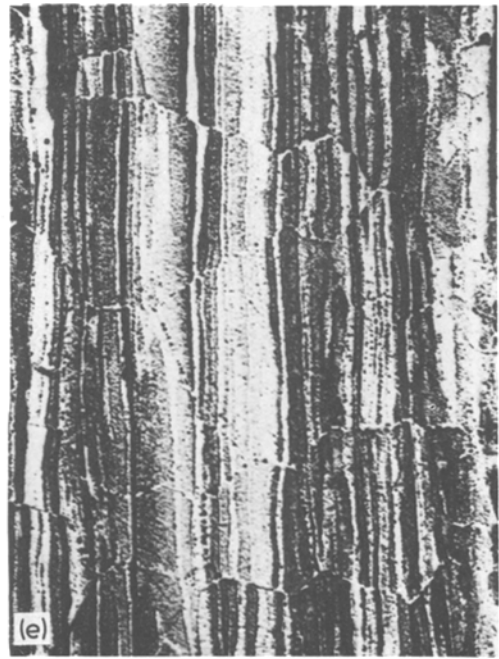


Figure 1 continued

gen at 550°C for 12 h, resulting in the microstructure shown in Fig. 1a and b. The annealing treatment produced a finely dispersed zirconium hydride precipitate [7, 8] and resulted in a grain size of 95 to 110 μm .

The annealed bar was then machined into creep samples with a rectangular cross section 5 mm \times 12.5 mm and a shoulder-to-shoulder length of 40 mm. The two largest surfaces were polished to a 4 to 8 μm diamond powder finish and the scratches remaining used as one set of marker lines. Two other sets were placed on the surfaces at an angle of 45 to 50° on each side of the stress axis. The surface of a sample after testing is shown in Fig. 1c. Multiple sets of marker lines are necessary since two sets must intersect each grain boundary in order to determine relative grain displacements produced by DC [1].

The creep tests were carried out at 450°C ($T/T_m = 0.78$) under constant load in a static argon atmosphere. The two samples for which data are reported were tested at loads of 4.57 and 6.55 MPa. The grain sizes of these samples were 106 and 95 μm , respectively. These samples were selected to show predominately DC and RC behaviour.

A threshold stress (i.e. no strain was detected for periods of up to 50 h at lower stresses) of about 2.25 MPa was found at 450°C, therefore the

effective stress for DC is approximately 2.3 MPa. It will be shown in the following sections that the low stress sample deformed by DC while the high stress sample had no DC strain component.

The minimum creep rates for the RC and DC samples were 3.19×10^{-6} and $3.54 \times 10^{-7} \text{sec}^{-1}$, respectively. The creep rate for the DC sample began to increase at 5 to 6% strain apparently because of the formation of voids at transverse grain boundaries; the test was stopped at that point. The RC test was stopped at about the same strain so that measured parameters would be roughly comparable. The total strains were 4.91 and 6.57% for the RC and DC samples, respectively.

Photomicrographs of the surfaces of the tested samples were projected to obtain the 800 to 1000 \times magnification necessary for measurement of the marker line offsets. The sliding and apparent diffusional components of the relative grain displacements (see Fig. 2) were determined from the marker line offsets by the method presented previously [1].

In order to reveal the hydride stringers which acted as marker lines on interior sections, samples were polished after creep and etched in a solution containing 5 g malic acid 2 cm³ nitric acid, 0.5 cm³ hydrochloric acid and 97.5 cm³ ethanol [9] (Fig. 1d and e). This also revealed, as precipitate-free

zones, the diffused material at the boundaries where material has “plated out” (Fig. 1d).

The extent to which sliding and diffusion contribute to the total displacement vector is the subject of current debate [3–5, 10]. The two possible configurations are illustrated in Fig. 2, a donor and an acceptor boundary being shown for both cases. A donor boundary is one which loses material (vacancy sink) and an acceptor boundary gains material (vacancy source) [2].

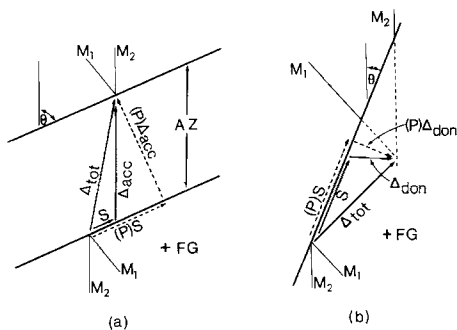


Figure 2 Showing relationships between total relative displacement Δ_{tot} at a grain boundary and the components for diffusion Δ and sliding s , for (a) acceptor and (b) donor boundary (see text). The diffusional components shown are based on alternative definitions: solid arrows – components parallel and perpendicular to stress axis [5]; dotted arrows – components perpendicular to grain boundaries [3]. FG – fixed grains; AZ – acceptor zone; M – marker line. Stress axis vertical.

If the displacement vectors are broken down as shown by the solid arrows in Fig. 2 the diffusional component is parallel or perpendicular to the stress axis for acceptor or donor boundaries, respectively, and the sliding component s is parallel to the grain boundary for both boundary types. Note that in this case the sliding component for the acceptor boundary is the same as that obtained from the offset of the set of marker lines parallel to the stress axis. This is usually represented by w , the offset measured perpendicular to the marker lines, a parameter often used to monitor GBS. For the marker line configuration used here there is no single offset which yields s for a donor boundary (this could be done with marker lines perpendicular to the stress axis).

The value of s obtained for an acceptor boundary, when the diffusional component is chosen parallel to the stress axis, is related to w by

$$w = s \sin \theta. \quad (1)$$

Note that this is only true for this case; under the alternative assumption that the diffusional component is perpendicular to the grain boundary [3] the sliding component for an acceptor boundary is not given by Equation 1.

The diffusional and sliding components presented here were calculated according to the convention illustrated by solid arrows in Fig. 2 as this configuration appears to be more nearly representative of the behaviour of an actual polycrystalline material* than that illustrated by dotted arrows [5].

2.2. Results

2.2.1. Sliding components s and w

Measurements of s and θ , and hence of values of w , were made and grouped into averages for 10° intervals of θ ; this grouping is used throughout the paper. As in most previous work, negative sliding was not distinguished i.e. the total sliding was assessed without regard to sign.

s and w as functions of θ are shown for the RC specimen in Fig. 3a, and for the DC specimen in Fig. 3b. For the latter the internal measurements gave results only in the range 30 to 90° , because the stringers did not sample boundaries with $\theta < 30^\circ$ adequately, as did the three sets of marker lines available for the surface measurements.

There is a further difficulty in using the stringers to measure s , which arose because of their irregular shape (see Fig. 1b). As a result sliding movements which produced offsets normal to the surface of section there could be uncertainties in matching of the two halves of the stringers and thus indeterminate errors in s .

Another error in the internal measurements occurred at $\theta = 30$ to 40° , for in this range a significant number of donor boundaries were present (see later, Fig. 4b, which shows the proportion to be approximately 50%). The donor component produces an offset which is indistinguishable from a true sliding offset (see Fig. 2). A correction to the internal sliding value at $\theta = 30$ to 40° in Fig. 3b has been made using the measured apparent diffusional component and percentage of donor boundaries (see Fig. 4b later). No correction was required for $\theta > 40^\circ$ because the proportion of donor boundaries is then small, as will emerge when measurements of these are reported in the next Section (also see Fig. 4b).

* It should be noted that the total relative displacement vector may be produced entirely by diffusion, i.e. it is possible that during DC no GBS, occurring by a distinct mechanism as during RC, takes place [2].

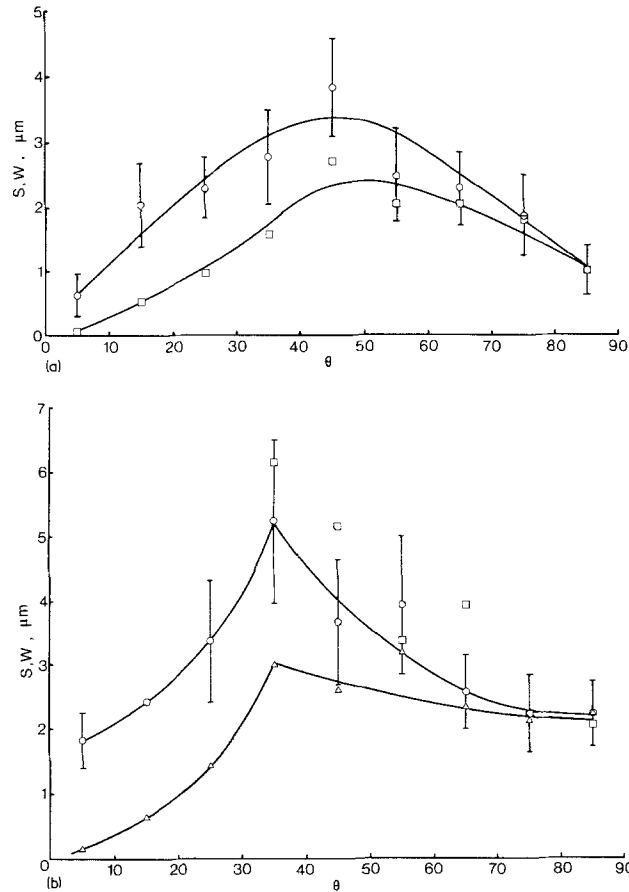


Figure 3 Sliding components s and w as a function of grain-boundary angle θ . (a) RC specimen; surface measurements; $\circ - s$ and $\square - w$. (b) DC specimen; surface measurements; $\circ - s$ and $\triangle - w$; internal measurements $\square - s$.

2.2.2. Apparent diffusional components

Using the convention illustrated by the solid arrows in Fig. 2, apparent diffusional components Δ_{acc} and Δ_{don} (at the acceptor and donor boundaries, respectively) can be measured [1] and are shown in Fig. 4a and b.* These are designated “apparent” because they may contain a contribution from the sliding which takes place normal to the surface and which is measured by v . The apparent diffusional components are corrected for the v contribution to obtain the true diffusional components by the procedure presented in Section 3.2. It should be noted that in the RC case no boundaries should be mechanically identifiable as acceptor boundaries; however, it is convenient to use this designation in the following description of the processing of the raw data.

* A consistent notation has been used in this paper, whereby the symbol Δ indicates an *apparent* diffusion component, corresponding to an *actual* component D ; the symbol (P) indicates that the component it precedes has been resolved perpendicular to the grain boundary. The subscripts “acc” and “don” refer to components at “acceptor” and “donor” boundaries (as defined in Section 2.1) and the subscript “ v ” indicates that a component has been derived from the “vertical” (v) measurements of GBS.

In order to obtain mean values of diffusional components for each range of θ it is necessary to convert the components Δ_{acc} and Δ_{don} into components perpendicular to the grain boundary (P) Δ_{acc} and (P) Δ_{don} . Acceptor and donor components are simply related:

$$(P)\Delta_{\text{acc}} = \Delta_{\text{acc}} \cdot \sin \theta \quad (2)$$

$$\text{and} \quad (P)\Delta_{\text{don}} = \Delta_{\text{don}} \cdot \cos \theta. \quad (3)$$

One further piece of information is required in order to calculate mean values, namely the proportion of boundaries of each kind in each range of θ . The (upper) inserts in Fig. 4a and b show the fraction of acceptor boundaries f_{acc} and those having zero diffusional component; the remainder are then donor boundaries f_{don} .

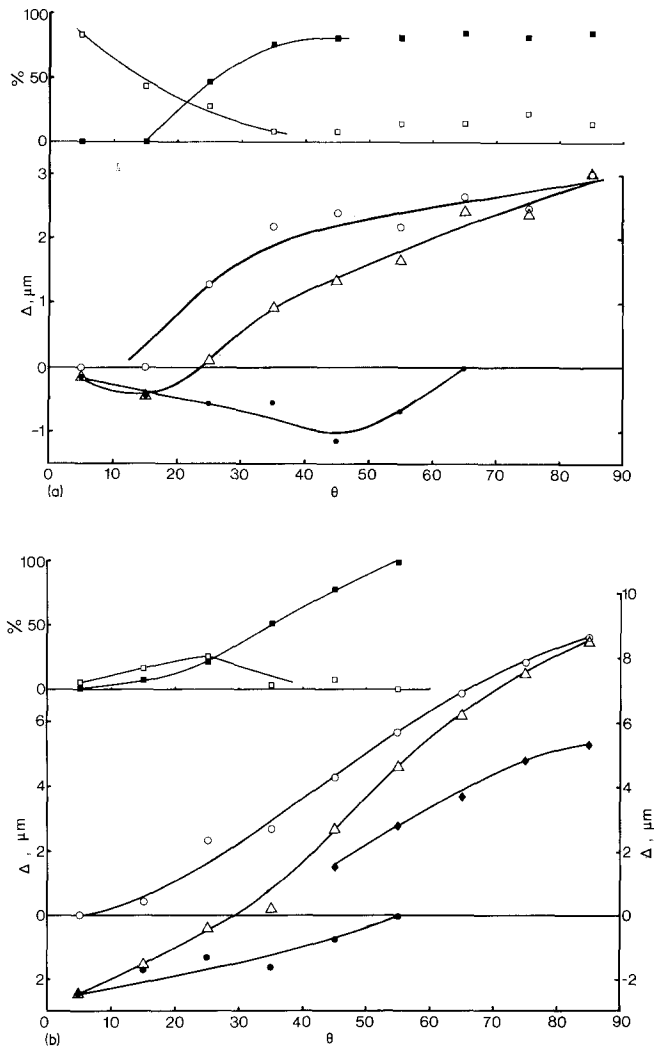


Figure 4 Diffusional components (lower diagrams) and grain-boundary types (upper diagrams) as functions of θ . (a) RC specimen, $\circ - \Delta_{acc}$, $\bullet - \Delta_{don}$, $\triangle - (P)\Delta$ (lower), $\square -$ no change, $\blacksquare -$ acceptor boundary (upper). (b) DC specimen, $\circ - \Delta_{acc}$, $\bullet - \Delta_{don}$, $\triangle - (P)\Delta$ and $\blacklozenge - (P)D_{acc}$ (lower), $\square -$ no change, $\blacksquare -$ acceptor boundaries (upper).

Next, by multiplying the appropriate values of $(P)\Delta_{acc}$ and $(P)\Delta_{don}$ by those fractions and algebraically summing, the mean apparent diffusional component perpendicular to the grain boundaries, $(P)\Delta$, is obtained:

$$(P)\Delta = f_{acc}(P)\Delta_{acc} - f_{don}(P)\Delta_{don}. \quad (4)$$

This is plotted as a function of θ for the RC and DC cases in Fig. 4a and b, respectively.

2.2.3. Widths of precipitate-free zones

Values of the true diffusional component for the DC specimen were also found by measurement of the width of precipitate-free zones at acceptor boundaries directly on the etched section. Since

the annealed specimens before creep had precipitate-free zones of $1.8\mu\text{m}$ mean width (see Fig. 1a) this was subtracted from the measured values after creep to obtain the true diffusional component, $(P)D_{acc}$, plotted against θ in Fig. 4b. Precipitate-free zones were seldom found at boundaries with $\theta < \text{approximately } 40^\circ$, consequently values of $(P)D_{acc}$ were not obtained for these boundaries.

2.2.4. v , sliding component

Relative displacements at grain boundaries in a direction perpendicular to the specimen surface, v , were determined from the change in the "in focus" microscope position across the grain boundary.

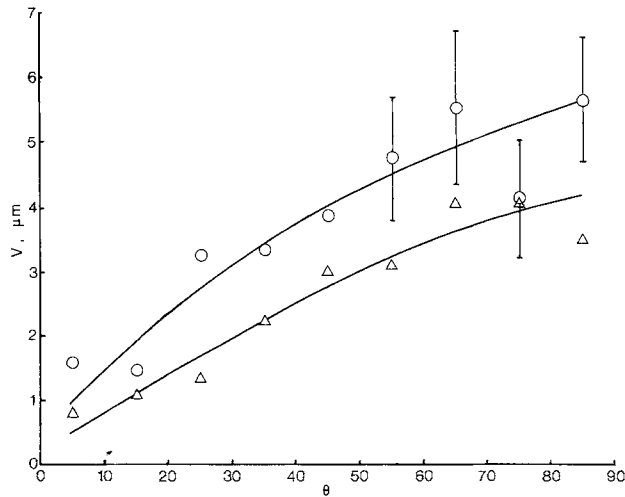


Figure 5 Vertical sliding steps v as a function of θ . Δ – RC specimen, \circ – DC specimen.

The results, averaged over each 10° interval, are plotted against θ in Fig. 5.

2.2.5. Grain-boundary angular frequency distributions

In order to employ the results obtained here to determine the contribution of diffusion and GBS to the total strain it is necessary to know the angular frequency distribution of the grain boundaries with respect to the stress axis (see Section 3.4). Measurements were made on the surfaces of both specimens after creep and on the interior of the DC specimen after creep. The resulting frequency f versus θ distributions are shown in Fig. 6. No significant difference is apparent between specimens or between surface and interior of the DC specimen. These distributions may be compared to that expected for a random (isotropic) structure also shown in Fig. 6, where the probability of intersection is proportional to $\sin \theta$.

2.2.6. Grain shape

Since grain shape is an important factor in DC, measurements were made to establish the degree of shape anisotropy of the grain structure. The average length to width ratio of grains $\overline{L/W}$ in the as-annealed condition was measured. Length and width were measured parallel and perpendicular to the extrusion axis, respectively. This ratio provides a statistically more significant result than the ratio of grain size measured in the two orthogonal directions [11]. A value of $\overline{L/W}$ of 1.088 ± 0.078 at the 95% confidence level was obtained.

2.2.7. Dihedral angles

The anisotropy of the grain structure indicates that the average angle between grain-boundary traces on the sample surface is not 120° as expected for an isotropic structure. As these angles are important in the calculation of the angular distribution of sliding (see Section 3.1) one set of

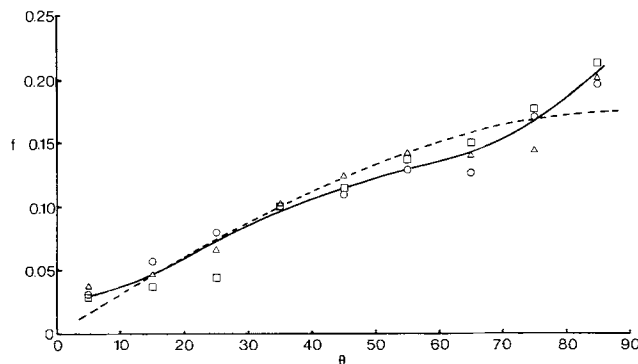


Figure 6 Frequency f of occurrence of grain-boundary trace angle θ on longitudinal traverses. DC specimen, \circ – surface, Δ – interior. RC specimen, \square – surface. The dotted curve shows the distribution expected for a random structure.

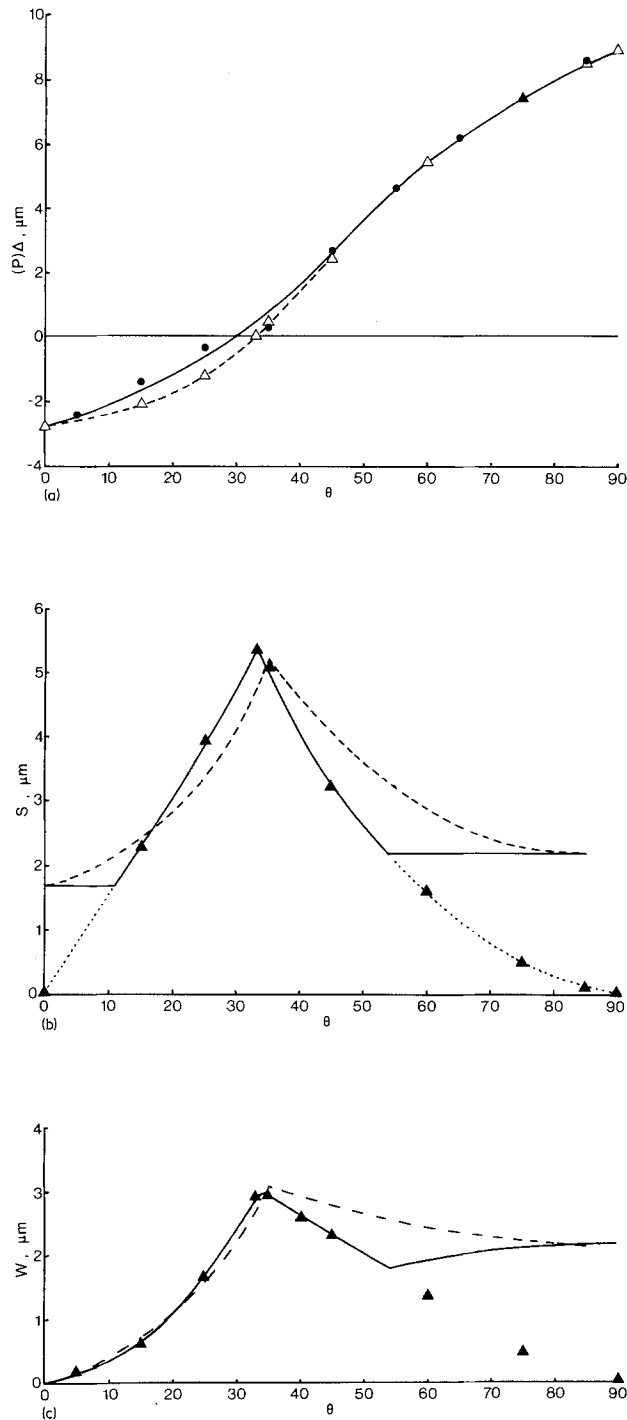


Figure 7 DC specimen; evolution of calculated curve for sliding components. (a) Experimental values of apparent diffusional component $(P)\Delta$ (solid circles and line) and values of $(P)\Delta$ (triangles and dotted curve) which were used for calculation of sliding component s (see Appendix), under the condition that $\theta = 32.3^\circ$ boundaries are incident on $\theta = 90^\circ$ boundaries. (b) Comparison of experimental (dashed) and calculated (solid) curves for s . The horizontal portions of the calculated curve are obtained by allowing for the non-ideal grain structure. (c) Comparison of experimental (dashed) curve and the (solid) curve for w converted from that for s in (b).

angles was measured as follows.

The angle that grain boundaries lying at 80 to 90° to the stress axis ($\theta = 80$ to 90°) make with adjacent boundaries was measured for 200 boundaries for the DC sample. The angle was found to be $122.26 \pm 1.81^\circ$ at 90% confidence. Thus the average value of θ for boundaries meeting an 80 to 90° boundary is $122.26 - 90 = 32.3^\circ$ rather than 30° as expected for a random structure.

3. Discussion

3.1. Comparison of the characteristics of GBS during DC and RC

As observed by Gifkins *et al.* [12] the w versus θ curve under RC conditions has a characteristic shape which can be accounted for by assuming that shear stress on the grain boundaries controls GBS. Their results for four different materials tested under RC conditions exhibit the same w versus θ behaviour as the RC data of Fig. 3a the salient feature in each case being the appearance of a maximum in the $\theta = 40$ to 50° range.

In the RC case the shear-stress control of sliding can be related to a model in which the sliding generated by the shear stress on a boundary is accommodated by a similarly oriented shear, e.g. in the form of a triple-point fold. In contrast, GBS under DC conditions can be viewed as accommodating the diffusional step, which results from the components of the applied stress normal to the grain boundaries. As pointed out by Gifkins and Langdon [2] this would be expected to lead to a different angular distribution of sliding from the RC case.

The distribution of the points shown for DC in Fig. 3b does not at first sight appear to be significantly different from the RC case in Fig. 3a, although the maximum value does appear to be in the $\theta = 30$ to 40° rather than 40 to 50° range. It can be shown that this difference in position of the maximum is significant by calculating the sliding component s from the diffusional component $(P)\Delta$. Details of this calculation are given in the Appendix. It is based on the angular distribution of $(P)\Delta$ shown in Fig. 4b and on the assumption that the average dihedral angle is 120°. As shown in the Appendix this was found to give reasonable agreement between calculated and experimental values of s . Some improvement in the agreement was obtained by using the measured value of 32.3° for the average value of θ for boundaries meeting $\theta = 80$ to 90° boundaries; all

other boundaries were assumed, as in the Appendix, to be at 120° to each other. Results for this case are shown in Fig. 7. It is likely that further improvement would be obtained if all the true average angles between grain-boundary traces were known.

The agreement between the experimental and calculated distributions of w versus θ for the DC case (Fig. 7c) indicates that the position of the maximum in the s versus θ curve for DC and the distribution of s is that drawn in Fig. 3b. This cusped curve is in strong contrast to the shear-stress case (Fig. 3a).

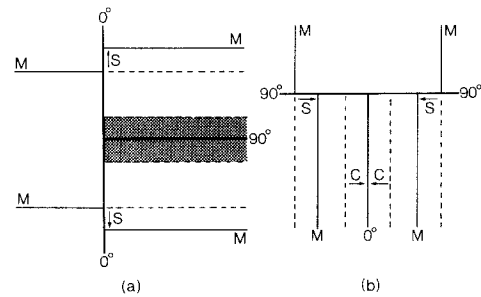


Figure 8 Illustrating schematically sliding produced by diffusion. (a) $\theta = 0$, accretion of material (shaded) at acceptor boundary. (b) $\theta = 90^\circ$, collapse at a donor boundary. M = marker line, S = sliding, C = collapse.

It was pointed out by Gifkins and Langdon [2] that an easily recognized difference in the angular distributions for the two kinds of creep should appear for the $\theta = 0$ and 90° boundaries. As illustrated in Fig. 8 a non-zero value of s should be present in the case of DC while for RC the shear stress is zero on these boundaries and so s should be zero. This difference can be detected if the present data are normalized as s/\bar{s} , \bar{s} being the average of s over the entire range of θ ($\bar{s} = 3.06$ and $2.15 \mu\text{m}$ for DC and RC, respectively). The difference between the two kinds of creep is significant at the 96% confidence level in the 0 to 10° range of θ ($s/\bar{s} = 0.59 \pm 0.13$ and 0.29 ± 0.14 for DC and RC, respectively). In the 80 to 90° range of θ the difference is not significant, probably because there is a large contribution of v to s which masks the effect.

3.2. Calculation of D , the true diffusional component from Δ , the apparent diffusional component.

Further differences between the two specimens are found when the true diffusional components D are

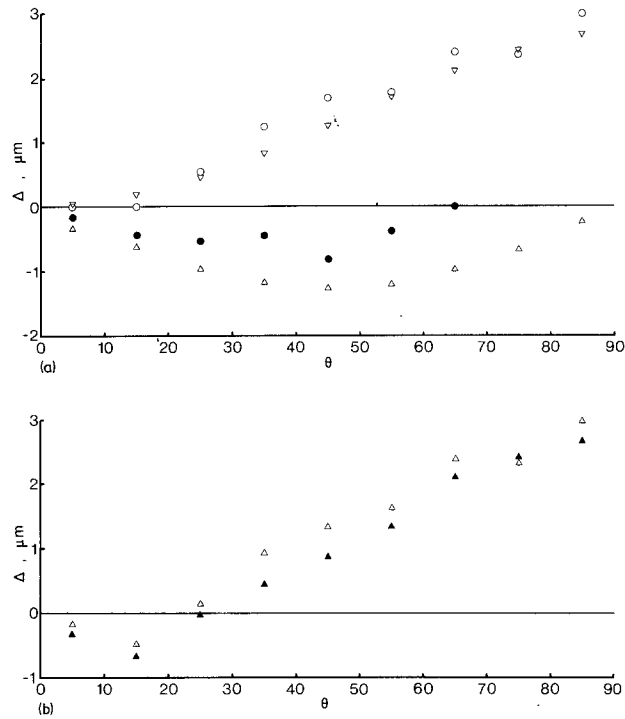


Figure 9 Comparison of experimental and calculated apparent "diffusional" components for the RC specimen, showing absence of diffusion. (a) experimental: $\circ - (P)\Delta_{acc}$ and $\bullet - (P)\Delta_{don}$, calculated: $\nabla - (P)\Delta_{v acc}$ and $\triangle - (P)\Delta_{v don}$; (b) experimental: $\triangle - (P)\Delta$, calculated: $\blacktriangle - (P)\Delta_v$.

compared; so far only values of the apparent diffusional components Δ have been considered.

If the grain boundaries are not normal to the sample surface, as in the case of an as-cut surface, the GBS component normal to the sample surface v produces an apparent diffusional component. When the experimental method employed here was proposed [1] it was expected that, during the relatively long time necessary for the DC tests, grain boundaries incident on the sample surface would migrate to form angles approaching 90° (an annealed surface) as had been observed previously [13–16]. When this is the case, the apparent diffusional component produced by v offsets is expected to be small enough that it can be neglected [1].

For the magnesium alloy used here the zirconium hydride precipitate prevents migration and hence rotation of grain boundaries within the duration of the DC tests. Therefore, the effect of v offsets on the apparent diffusional component must be considered. Correction for the v contribution was made as follows.

The apparent diffusional component Δ was calculated from the marker line offsets according to the method described elsewhere [1]. The

apparent diffusional component produced by the v sliding component Δ_v was calculated from the values of v shown in Fig. 5, using the relation

$$\Delta_v(\theta) = v(\theta) \overline{\tan \alpha} \quad (5)$$

where $v(\theta)$ is the average value of v for a particular θ range. Note that the mean value of $\tan \alpha$ must be used, not the tangent of the mean value of α (the angle between the surface and a grain boundary trace on a section normal to the surface). The hydride precipitate prevented migration in the present specimens and the probability of occurrence of a value α then varies as $\sin \alpha$ and it can be shown that $\overline{\tan \alpha} = 0.637$

The values of Δ_v so found were assumed to be parallel to the stress axis for acceptor boundaries and perpendicular to the stress axis for donor boundaries. These values for the RC specimen, resolved normal to the grain boundaries are shown in Fig. 9a, together with the experimental values of the related apparent diffusional components, $(P)\Delta_{acc}$ and $(P)\Delta_{don}$.

Processing these data further by weighting according to the percentages of acceptor and donor boundaries present (Fig. 4a) and summing algebraically yields values of the apparent average

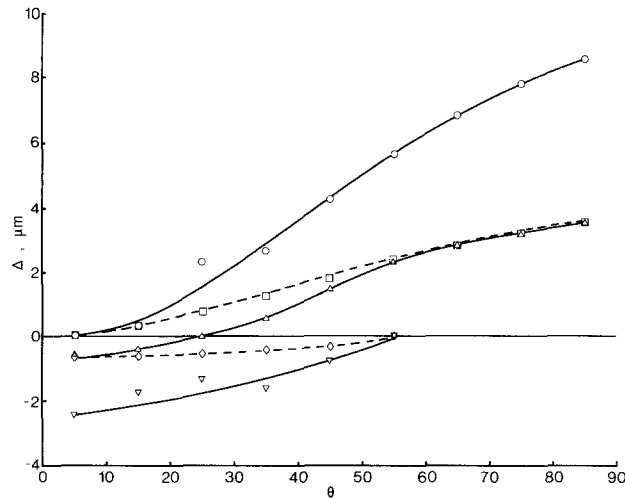


Figure 10 Comparison of experimental and calculated apparent diffusional components for the DC specimen. $\circ - \Delta_{acc}$, $\nabla - \Delta_{don}$, $\square - (P)\Delta_{v acc}$, $\diamond - (P)\Delta_{v don}$, $\triangle - (P)\Delta_v$.

normal diffusional components produced by v , $(P)\Delta_v$, which are plotted against θ in Fig. 9b. The close agreement between $(P)\Delta$ and $(P)\Delta_v$ over the whole range of θ shows that the apparent diffusional component in the RC case is produced by the v -direction sliding, i.e. there is no true diffusional component. This is further illustrated in Fig. 11 where the values of $(P)\Delta - (P)\Delta_v$ for the RC specimen are plotted. The difference is zero to within experimental error.

Essentially the same procedure was used to calculate $(P)\Delta_v$ for the DC specimen, but the form of the dependence of Δ_{don} on θ being different (see Figs. 9a and 10) there was a difference in detail. For the DC case Δ_{don} decreases in magnitude with increasing θ , rather than increasing initially as for the RC specimen (see Fig. 4a and b); $\Delta_{v don}$ is assumed to follow the same trend. Therefore, the value of $\Delta_{v don}$ at $\theta = 0$ to 10° was calcu-

lated according to Equation 5 and the remaining values of $\Delta_{v don}$ calculated as the same fraction of Δ_{don} as at $\theta = 0$ to 10° . The values of $(P)\Delta_{v don}$ shown in Fig. 10 were obtained in this way.

As before, the values of $(P)\Delta_{v acc}$ and $(P)\Delta_{v don}$ were averaged, using the percentages of acceptor and donor boundaries (Fig. 4b) and summed algebraically giving the values of $(P)\Delta_v$ shown in Fig. 10. The true diffusional component $(P)D$ was then $(P)\Delta - (P)\Delta_v$ (values of $(P)\Delta$ being taken from Fig. 4b) which is plotted against θ in Fig. 11. It is clear that in the DC case there is a significant true diffusional contribution.

3.3. Comparison of surface and internal measurements

The data obtained by the surface marker line method were checked by comparison with the measurements on the interior of the DC specimen.

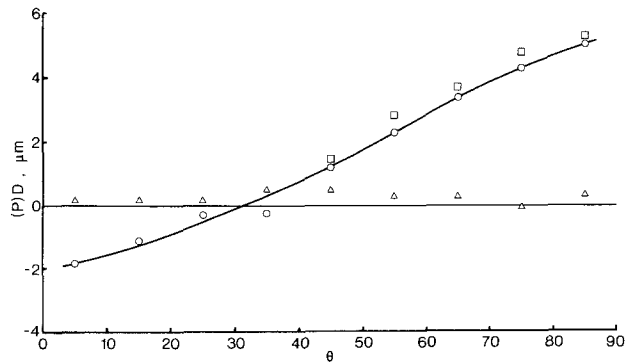


Figure 11 Comparison of true diffusional components $(P)D$ for RC and DC specimens. $\square - (P)D$ for DC specimen determined from corrected thickness of precipitate-free zones at acceptor boundaries. $\circ - (P)D = (P)\Delta - (P)\Delta_v$ for DC specimen, surface. $\triangle - (P)D = (P)\Delta - (P)\Delta_v$ for RC specimen, surface.

The GBS data from hydride stringer offsets agree reasonably well with the surface data as shown in Fig. 3b.

Precipitate-free zone thickness, corrected for as-annealed zone thickness, is plotted again in Fig. 11 for comparison with the surface data.

The general agreement between surface and interior measurements is good indicating; (i) that the experimental technique based on offset measurements of surface marker lines is satisfactory and, (ii) that, at least for the magnesium alloy investigated here, the surface and interior grains undergo the same relative displacements during DC.

3.4. Strains contributed by sliding and diffusion

It has been shown that the most reliable relationship between surface measurements of GBS and strain contributed by GBS ϵ_{gb} is [17, 18]

$$\epsilon_{gb} = 2N_1(1 + \epsilon_t) \overline{[w/\tan \theta]}_1 \quad (6)$$

where N_1 is the number of grain boundaries per unit length of test line parallel to the stress axis after creep, ϵ_t the total strain, w the marker line offset (of marker lines parallel to the stress axis) measured perpendicular to the stress axis and θ the angle between grain boundaries and stress axis. $\overline{[w/\tan \theta]}_1$ is the average value of $w/\tan \theta$ for boundaries sampled by a longitudinal line (parallel to the stress axis). Equation 6 is strictly applicable only to internal offset data; however, since the agreement between surface and internal sliding data is good for the DC sample and because the surface data have a smaller statistical error, they have been used here to calculate ϵ_{gb} .

The component of s parallel to the stress axis s_1 is equal to $w/\tan \theta$. The average value of s_1 , found by sampling with a longitudinal traverse, is given by

$$\overline{s}_1 = \sum_{\theta} f(\theta) \cdot s_1(\theta) \quad (7)$$

where $f(\theta)$ is the frequency of θ values as a function of θ , found by sampling with a longitudinal test line. These factors are shown by the solid curve in Fig. 6. When Equation 7 is applied to the DC data a value of $1.69 \mu\text{m}$ is obtained for \overline{s}_1 . N_1 (after creep) is 94 cm^{-1} and ϵ_t is 6.57%. With these values Equation 6 gives 3.38% for ϵ_{gb} .

The strain produced by the diffusional com-

ponents ϵ_d is given by

$$\epsilon_d = N_1(1 + \epsilon_t) \overline{D}_1 \quad (8)$$

where

$$D_1 = \sum_{\theta} f(\theta) \cdot D_1(\theta). \quad (9)$$

$D_1(\theta)$ are the diffusional components parallel to the stress axis and, in terms of the measured $(P)D(\theta)$ data, are given by

$$D_1(\theta) = -(P)D(\theta) \sin \theta \quad (10)$$

for donor boundaries and

$$D_1(\theta) = +(P)D(\theta)/\sin \theta \quad (11)$$

for acceptor boundaries. With Equations 8 to 11, 3.17% was obtained for ϵ_d for the DC sample.

If sliding and diffusion are responsible for deformation in the DC case the sum of ϵ_{gb} and ϵ_d should give ϵ_t . The sum of the values calculated here 6.55% agrees with the measured ϵ_t of 6.57%; thus diffusion and the GBS which accommodates it account entirely for the deformation of the DC specimen.

The ratio $\gamma = \epsilon_{gb}/\epsilon_t$ for the DC specimen is 0.51. It should be noted that the values of ϵ_{gb} , ϵ_d and hence γ depend upon how the diffusional and sliding components are chosen. As mentioned previously, here the diffusional component has been taken parallel to the stress axis rather than perpendicular to the grain boundary (see Fig. 2). The latter convention gives a larger ϵ_{gb} contribution than the former and thus for the DC specimen increases γ to 0.68. This compares reasonably well with values of 0.62 to 0.63 calculated by Stevens for tetrakaidecahedra and dodecahedra [3] with the convention that the diffusional component is perpendicular to the grain boundary. It must be emphasized that this agreement is a result of processing the experimental results according to Stevens' convention. It is not, therefore, a proof of the validity of this convention. Appeal to other arguments must be made to decide this question [5].

It is expected that γ will be about the same as the value of 0.5 found here in all cases of DC. This is because the dependence of both $(P)D$ and s on θ is fixed by the grain shape. Thus γ does not vary with stress, temperature or grain size but only with grain shape under DC conditions.

For the RC sample ϵ_{gb} was also calculated using Equations 6 and 7. The value of \overline{s}_1 is $1.23 \mu\text{m}$ and for $\epsilon_t = 4.91\%$ and $N_1 = 105 \text{ cm}^{-1}$, hence, ϵ_{gb} is

2.72%. γ in this case is 0.55. This is a rather high value for RC; however, the precise mode of creep for this specimen has not been established, the designation recovery creep being based on analogy with the work of Burton and Greenwood on copper [6]. It is likely that there is at least a strong component of some other regime of creep where other accommodating mechanisms could allow γ to be larger (see e.g. [19]).

As pointed out previously, the hydride precipitate anchors the grain boundaries and prevents grain growth and grain-boundary migration. Further indirect evidence for this, based on the GBS measurements, is as follows. The ratio of \bar{v}_1/\bar{w}_1 is unity in the sample interior as the v and w components are indistinguishable. However, at the surface this is not the case and \bar{v}_1/\bar{w}_1 is expected to vary from about 1 for an annealed surface to as high as 2 for an as-cut surface [12]. This is for the case of RC; however, the constraint conditions at the surface are the same for DC and thus similar behaviour is expected.

The values of \bar{v}_1/\bar{w}_1 obtained for the RC and DC cases are 1.96 and 1.94, respectively, values characteristic of an as-cut surface. This confirms that there has been little or no migration of grain boundaries at the surface to the annealed configuration.

4. Conclusions

(1) DC and RC exhibit distinctively different angular dependencies of GBS.

(2) The previously presented method for the measurement of DC [1], when modified as

described here, allows the determination of diffusional and sliding components for samples with either as-cut or annealed surface conditions.

(3) For the material investigated here the surface and interior grains exhibit the same sliding and diffusional changes (in the plane of the polished surface) under DC conditions.

(4) The value of 0.5 found for γ is a general characteristic of DC.

(5) The strain in a DC specimen is entirely accounted for by the measured diffusional and sliding contributions.

(6) No diffusional component could be detected in the RC case.

Appendix. Calculation of the s versus θ curve from (P) Δ versus θ data

Consider the (P) Δ versus θ curve for DC in Fig. 4b. If the only deformation mechanisms active in this case are diffusion and GBS then GBS must occur under the conditions that the motions indicated by (P) Δ versus θ occur and volume is conserved. Under these conditions and the assumption that the average angle at which grain-boundary traces meet on the surface is 120° the sliding components can be calculated. Three examples are as follows.

(1) Fig. 12a shows a boundary at 90° to the stress axis $\theta = 90^\circ$ incident on two $\theta = 30^\circ$ boundaries. Assume that the structure is ideal and all angles between grain-boundary traces are 120° . For a $\theta = 90^\circ$ boundary in an ideal structure s is zero and according to Fig. 13a (the (P) Δ versus θ curve for DC shown in Fig. 4b is reproduced here

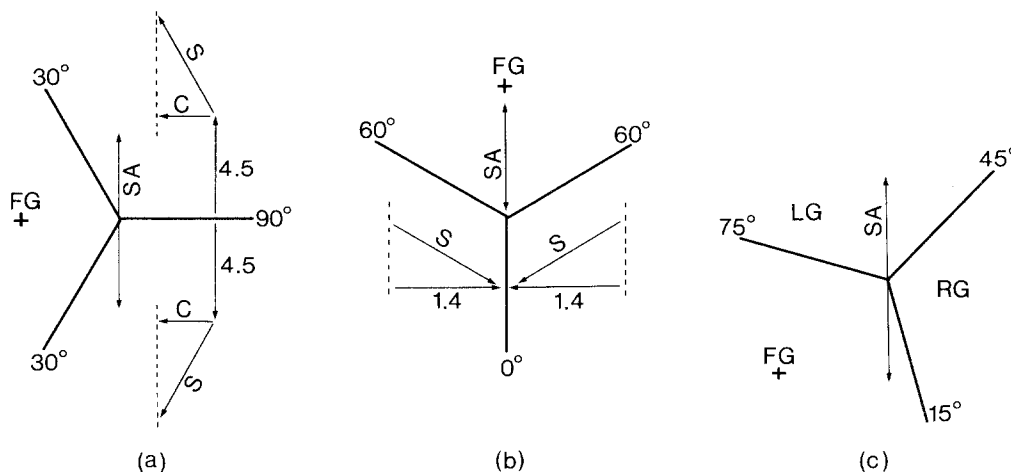


Figure 12 Triple-point configurations used in calculation of sliding during DC for values of θ . (a) 30° , (b) 60° and (c) 75° . LG, RG – left and right grain; FG – fixed grain; S – sliding; C – closure.

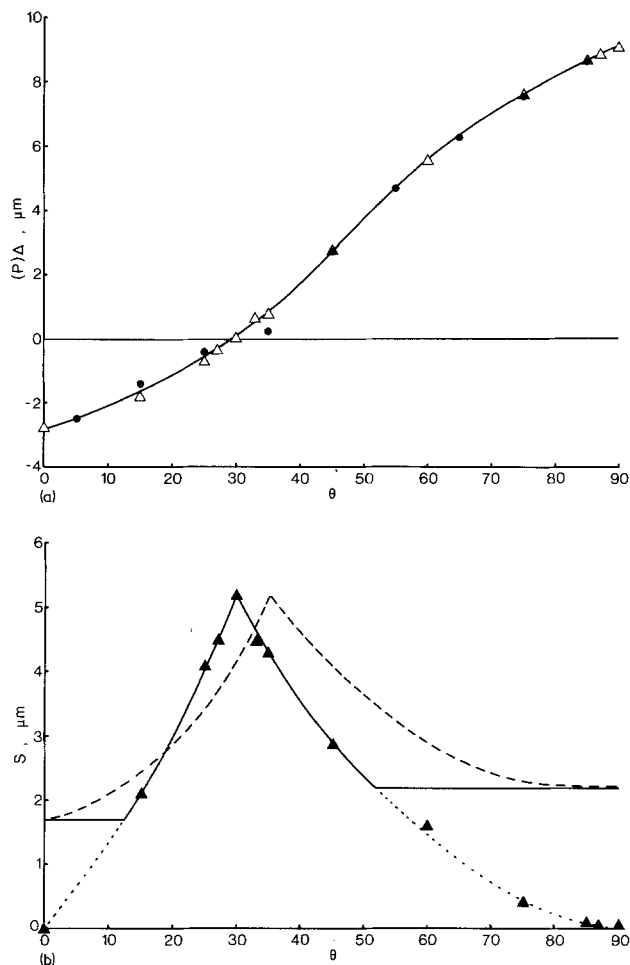


Figure 13 DC specimen; evolution of calculated curve for sliding components. (a) Experimental values of apparent diffusional component $(P)\Delta$ (solid circles and line) and calculated values of $(P)\Delta$ (triangles) which were used for calculation of sliding component s , under the condition that all dihedral angles have an average value of 120° . (b) Comparison of experimental (dashed) and calculated (solid) curves for s . The horizontal portions of the calculated curve are obtained by allowing for the non-ideal grain structure.

for convenience) $(P)\Delta = 9.0\ \mu\text{m}$ at $\theta = 90^\circ$. This defines the motion across the 90° boundary. According to Fig. 13a $(P)\Delta = 0$ at $\theta = 30^\circ$. Sliding at the 30° boundaries must be such that its component parallel to the 90° boundary, labelled closure in Fig. 12a, closes the gaps created at the 30° boundaries by $(P)\Delta$ at the 90° boundary. Thus the two grains on the right must move to the left relative to the fixed grain to close the gaps. This motion produces an offset of marker lines at the 30° boundaries which appears as sliding of magnitude $4.5/\cos 30^\circ = 5.20\ \mu\text{m}$, as shown in Fig. 13b.

(2) Consider the configuration shown in Fig. 12b. As for the 90° boundary the $\theta = 0^\circ$ boundary in an ideal structure has zero sliding component. The $(P)\Delta$ values at 0 and 60° are again

obtained from Fig. 13a. The donor component of the 0° boundary produces marker line offsets at the 60° boundaries which appear as GBS of magnitude $1.4/\sin 60^\circ = 1.62\ \mu\text{m}$.

(3) The remaining sliding values must be "balanced" as illustrated by the third sample shown in Fig. 12c. The values of s for the 15 and 75° boundaries are roughly established from curves through the sliding values at $\theta = 0, 30, 60$ and 90° calculated above. The motions of the left and right grains relative to the fixed grain are then known which establishes the total displacement for the 45° boundary. The 45° $(P)\Delta$ component must lie on the curve in Fig. 13a. The 15, 45 and 75° s components are adjusted so that smooth curves result between the 0, 30, 60 and 90° s values.

The s values calculated in this way are shown in Fig. 13b and the corresponding (P) Δ values in Fig. 13a. The curve established by the s data in Fig. 13b reaches a maximum at $\theta = 30^\circ$ and is zero at $\theta = 0^\circ$ and 90° . This is in contrast to the experimental data which reach a maximum at a somewhat higher value of θ and are not zero at $\theta = 0$ and 90° . These discrepancies are probably due to the non-ideality of the grain structure. The non-zero values at $\theta = 0$ and 90° are accounted for as follows.

If the s versus θ based on 120° dihedral angles (Fig. 13b) represents the ideal sliding behaviour, then a sliding term resulting from non-ideality of the structure s_{ni} must be added (or subtracted) from the ideal sliding component s_i to obtain the observed sliding component s .

$$s = s_i \pm s_{ni}. \quad (\text{A1})$$

The direction of s_{ni} relative to s_i is random, therefore s_{ni} produces an increase or a decrease with equal frequency. When $s_i = 0$, as at $\theta = 0$ or 90° , $s = \pm s_{ni}$. Since the measured sliding data were averaged irrespective of sign to obtain the experimental s values, $s = |s_{ni}|$ at $\theta = 0$ and 90° . For other values of θ , $s_i \neq 0$ and s can be expressed as

$$s = \frac{|s_i + s_{ni}| + |s_i - s_{ni}|}{2}. \quad (\text{A2})$$

For $|s_i| < |s_{ni}|$ this gives

$$s = \frac{s_i + s_{ni} + s_{ni} - s_i}{2} = s_{ni}$$

and for $|s_i| > |s_{ni}|$

$$s = \frac{s_i + s_{ni} + s_i - s_{ni}}{2} = s_i.$$

Therefore, for θ values where $|s_i| < |s_{ni}|$, $s = s_{ni}$, and for θ values where $|s_i| > |s_{ni}|$, $s = s_i$.

If the experimental values of s at $\theta = 0$ and 90°

are taken as s_{ni} at these θ values the result is the "tails" to the curves shown in Fig. 13b. When this is combined with the ideal 120° angle curve the solid curve in Fig. 13b results.

The agreement between the position of the maximum in the experimental and calculated s versus θ curves can be improved by taking the true dihedral angles into account as shown in Section 3.1.

References

1. E. H. AIGELTINGER, *J. Mat. Sci.* **9** (1974) 644.
2. R. C. GIFKINS and T. G. LANGDON, *Scripta Met.* **4** (1970) 563.
3. R. N. STEVENS, *Phil. Mag.* **23** (1971) 265.
4. W. R. CANNON, *ibid* **25** (1972) 1489.
5. R. C. GIFKINS, T. G. LANGDON and D. MCLEAN, *Met. Sci. J.* **9** (1975) 141.
6. B. BURTON and G. W. GREENWOOD, *ibid* **4** (1970) 215.
7. J. E. HARRIS, P. G. PARTRIDGE, W. T. EELES and G. K. RICHARDS, *J. Nuclear Mat.* **9** (1963) 339.
8. J. E. HARRIS and P. G. PARTRIDGE, *J. Inst. Metals* **93** (1964-65) 15.
9. R. L. SQUIRES, R. T. WEINER and M. PHILLIPS, *J. Nuclear Mat.* **8** (1963) 77.
10. D. MCLEAN, *Met. Sci. J.* **4** (1970) 144.
11. J. H. HENSLER and R. C. GIFKINS, *J. Inst. Metals* **81** (1952-53) 33.
12. R. C. GIFKINS, A. GITTINS, R. L. BELL and T. G. LANGDON, *J. Mater. Sci.* **3** (1968) 306.
13. C. S. SMITH, "Metal Interfaces" (Amer. Soc. Metals, Cleveland, Ohio, 1952) p. 80.
14. R. C. GIFKINS, *Trans. Met. Soc. AIME* **215** (1959) 1015.
15. A. GITTINS and R. C. GIFKINS, *Met. Sci. J.* **1** (1967) 15.
16. T. G. LANGDON, *Trans. Met. Soc. AIME* **3** (1972) 797.
17. R. L. BELL, C. GRAEME-BARBER and T. G. LANGDON, *ibid* **239** (1967) 1821.
18. R. C. GIFKINS, to be published in *Met. Trans.* **505**.
19. R. C. GIFKINS, to be published.

Received 21 March and accepted 21 April 1975.